HSGPS Signal Analysis and Performance under Various Indoor Conditions

G. LACHAPELLE, H. KUUSNIEMI*, D. T. H. DAO, G. MACGOUGAN, and M. E. CANNON
Department of Geomatics Engineering, University of Calgary, Calgary, Alberta, Canada

ABSTRACT: *High-sensitivity GPS (HSGPS) receivers permit GPS signal measurements to be acquired and tracked in certain indoor environments where this previously was not possible. However, solution reliability and accuracy are significantly degraded because of the nonavailability of some satellites, multipath errors, measurement noise associated with the low power of the remaining signals, and echo-only and cross-correlation signal tracking. The focus of this paper is on improving static-mode HSGPS positioning performance in terms of accuracy and reliability. Thus, various techniques, such as height fixing, simulation-based noise modeling, reliability testing in terms of fault detection and exclusion (FDE), and batch processing, are implemented. An XTrac-LP™ HSGPS evaluation kit, developed by SiRF Technologies Inc., is used to investigate some indoor environments by analyzing the fading and pseudorange error conditions. In addition, the measurements provided by the receiver are used to test the performance of the algorithms intended to improve the HSGPS positioning capability.*

INTRODUCTION

Conventional GPS theory is limited to applications with direct line-of-sight (LOS) signals and is not applicable to highly attenuated signal environments. Location-based services and the E-112 and E-911 mandates in Europe and the United States, respectively, call for navigation capability in degraded signal environments, such as urban canyons and indoors. The need for this capability has helped motivate the development of high-sensitivity GPS (HSGPS) receivers. With the ability to track weak signals, HSGPS offers higher availability and broader applicability compared with conventional GPS. However, HSGPS is associated with higher noise levels and multiple measurement fault sources ranging in magnitude up to kilometers in some cases, and thus requires special measurement processing to obtain a reliable solution.

In aviation applications, statistical receiver autonomous integrity monitoring (RAIM) is used for the detection and exclusion of a navigation failure. RAIM makes statistical consistency checks on the GPS measurements to detect a navigation failure [1]. Detecting a failure can potentially lead to a successful exclusion [2]. In this research, RAIM—i.e., statistical reliability testing—is regarded as lending itself to the failure detection and exclusion functions not only in traditional aviation applications, but also in personal positioning applications for the rejection of poor-accuracy pseudoranges.

This paper describes HSGPS performance under some indoor conditions and investigates methods for improving static solution reliability and accuracy. Two indoor environments are analyzed in detail—inside a residential garage and inside a commercial concrete and steel building. The test metrics used to describe the environments tested include fading and estimated pseudorange errors. Statistics based on these test metrics are shown using azimuth-by-elevation representations, which include the structural outline of the test environment, referred to here as pierce-point analysis. This method is very powerful for gaining better insight into GPS signal behaviour indoors. To assess pseudorange measurement errors, a position- and clock-constrained Kalman filter approach is used to estimate each pseudorange error directly. The range errors are caused by noise, multipath, echo-only signals, signal cross-correlation, and other interference. Noise can reach tens of meters depending on the signal attenuation. Thus, the pseudorange measurement noise versus signal power was examined using a Spirent STR6560 hardware GPS signal simulator.

Following the environment and error analysis, incremental algorithmic steps are taken in an attempt to improve the performance of HSGPS positioning in terms of accuracy and reliability. These steps include height fixing, the simulation-based noise modeling, reliability and integrity analysis in

*Visiting Ph.D. student from Tampere University of Technology, Finland.

terms of fault detection and exclusion (FDE), and batch processing of static-mode positioning.

The first section of this paper reviews HSGPS theory and the HSGPS receiver used in the testing. The second section analyzes the characteristics of indoor positioning in general in terms of fading and measurement errors, and also presents the indoor environments of the conducted tests using pierce-point analyses. Then in the next section, methods to improve HSGPS positioning accuracy and reliability performance are discussed. Subsequently, results of the conducted tests are shown and discussed. Finally, conclusions, remarks, and tasks for future work are presented.

THEORY OF HSGPS

The theory of HSGPS lies in the improved ability to acquire and track weak GPS signals. In general, to acquire GPS signals, coherent integration and non-coherent accumulation are performed to effectively increase the total signal dwell time. In general, the coherent integration period is limited to 20 ms because of the length of the navigation bits, as well as residual frequency errors during the coherent integration period. Residual frequency errors are caused by satellite motion, receiver clock instability, and user motion–induced Doppler effects [3]. The noncoherent integration period, which is the squared output of the coherent interval, can be much longer compared with the coherent integration. However, this procedure results in a squaring loss. Therefore, the acquisition and tracking of weak signals is a matter of maximizing the coherent integration interval and minimizing residual frequency errors.

A number of factors affecting HSGPS performance must be considered in designing the receivers. First, thermal noise should be minimized to maintain the tracking and avoid carrier-tracking error. The ability to predict a bit transition is important for obtaining a long coherent interval. Furthermore, the residual frequency error can be reduced by using a more stable oscillator. The total dwell time of HSGPS receivers can be up to hundreds of milliseconds, while it is less than the 20 ms coherent integration interval maximum for conventional GPS.

In general, high-sensitivity methods can be implemented in either aided (AGPS) or unaided modes. In aided mode, high-sensitivity receivers rely on assistance data including time, approximate position, satellite ephemerides, and possibly code differential GPS corrections. Massive parallel correlation is necessary to facilitate the complex task of searching for the weaker GPS signals while using long coherent integration periods and further noncoherent accumulation [4]. In unaided mode, a high-sensitivity receiver lacks the ability of an aided receiver to acquire weak signals if it has no a priori knowledge.

If the receiver is initialized with the same assistance data, however, by acquiring and tracking four or more GPS satellites with strong signals, it has the same functional capability as an assisted GPS receiver as long as it can maintain timing, approximate position, and satellite ephemeris.

TEST RECEIVER

The test receiver used was an XTrac-LP™ (Extended Tracking-Low Power) evaluation kit [5] provided by SiRF Technologies Inc. Some key receiver performance characteristics are provided in Table 1.

The HSGPS methodology used in this study was the unaided positioning approach. The receiver was first initialized for about 20 min through LOS tracking and then brought into the degraded signal environment.

INDOOR ENVIRONMENT CHARACTERIZATION

To analyze the performance of HSGPS, it is important to characterize signal degradation and error sources for indoor environments to understand the behavior of the signals.

Fading

The direct received GPS L1 C/A-code signal power is specified to be at least -160 dBW at 5 deg and 90 deg elevation angles, but will be as much as 2 dB higher at 40 deg elevation angles [6]. Indoors, building materials such as glass, concrete, steel, insulation, drywall, wood, and other materials attenuate the LOS signal. In addition, the received signal is composed of a combination of the LOS signal and reflections that cause constructive and destructive interference effects. It is therefore important to analyze how much degradation and interference is due to the surrounding environment.

Carrier-to-noise density ratio, or C/N_0, is the best measurable value of the signal quality present at the input to a GPS receiver. C/N_0 is an instantaneous measure of the ratio of carrier power present to noise power density measured per hertz of bandwidth. The nominal noise floor has a spectral density of approximately -204 dBW/Hz. With a minimum guaranteed LOS GPS signal power of -160 dBW, the nominal C/N_0 level is 44 dB-Hz. Theoretically, C/N_0 is irrespective of the receiver used; however, each receiver

Table 1 — XTrac-LP™ Receiver Characteristics

Tracking sensitivity*	-186.0 dBW
Reacquisition sensitivity*	-177.9 dBW
Temperature-compensated crystal oscillator (TCXO)	0.5 ppm
Total signal dwell time for weak signals	$340-800$ ms

*Determined by hardware simulation testing at the University of Calgary [3].

must compute its value based on the measured signal. Therefore, the C/N_0 ratio is not necessarily the best measure for assessing the impact of the environment on signal quality.

Signal strength degradation is due to two effects. The first is the attenuation of the LOS signal due to propagation through a material, often referred to as shadowing. The second effect is due to constructive and destructive interference when the GPS signal experiences interference, such as multipath. This effect is generally referred to as fading. For the purposes of this paper, however, fading refers to both the shadowing effect and the interference fading effect. The fading test measure is thus a measure of signal strength degradation and can be determined by differencing a test receiver's C/N_0 data with those from a reference receiver located nearby with LOS signal reception. Fading (dB) can thus be calculated as

$$F = C/N_0^{\text{reference}} - C/N_0^{\text{rover}}$$

The fading test metric is presented both temporally using time-domain analysis and spatially using pierce-point analysis. This is a very helpful way of looking at GPS signal behavior in a particular environment.

Estimated Pseudorange Error

To determine the extent to which multipath, noise, echo-only signals, and other interference degrade the pseudorange measurements taken at the test site, the test receiver's raw data can be postprocessed using an estimation technique in which the errors in the measurement to each satellite are estimated. A Kalman filter utilizing pseudorange and Doppler measurements is used with fixed position and constrained clock information to estimate these errors. This test metric is hence referred to as estimated pseudorange error (EPE). The position- and clock-constrained filtering is used to analyze the direct epoch-by-epoch errors in the pseudorange measurements without having the errors extend into the solution or the clock estimate. Kalman filtering can reduce the distortion of the EPE values as a result of error absorption by the receiver clock estimate [3].

Test Environment Description

Residential Garage

A test was carried out inside a residential garage (see Figure 1) over a time period of 12 h in June 2003. The inside of the garage is shown in Figure 2; during the test, the wooden garage door was closed. An HSGPS receiver and a NovAtel 600 antenna were used in the garage test for both the initialization and the indoor positioning. In addition, differential positioning mode was used to eliminate orbit

Fig. 1 – Residential Garage Used for Test

Fig. 2 – Inside View of Garage

and atmospheric errors, and a NovAtel OEM4 receiver system was used at a reference station that was set up approximately 5 km from the test site and had clear lines of sight to the satellites.

Fading conditions inside the garage are typical of PRN25, as shown in Figure 3. Figure 4 presents signal fading for all satellites during the test. To further investigate fading behavior, the C/N_0 data from all satellites were binned into 15 deg elevation
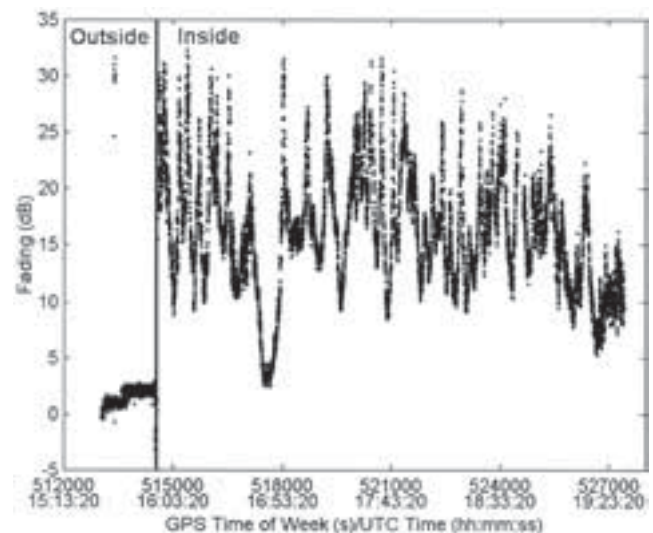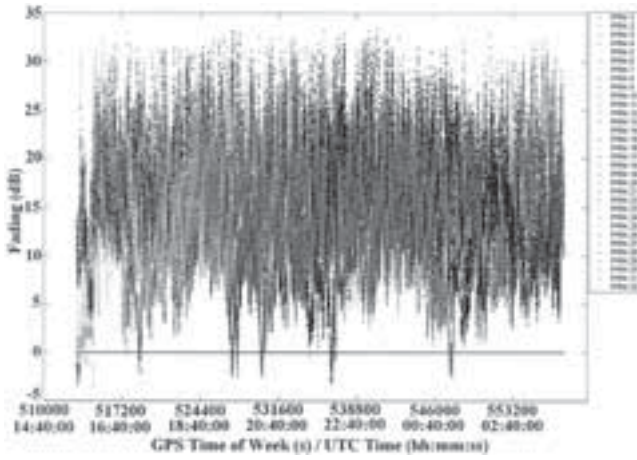

Fig. 3 – Signal Fading inside the Garage for PRN25

Fig. 4–Signal Fading for All Satellites: Garage

Fig. 6–Pierce-Point Analysis: HSGPS RMS Fading in the Garage
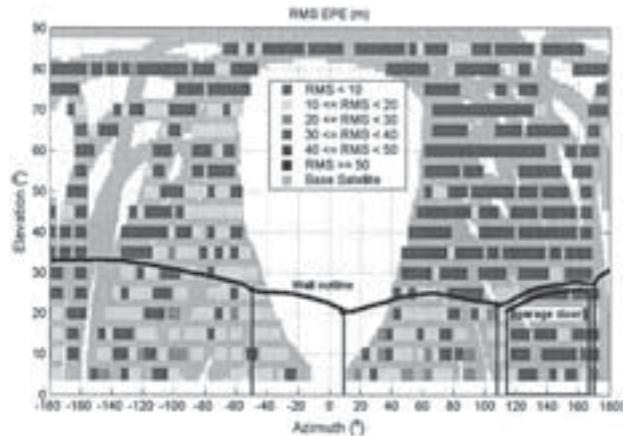
Fig. 7–Pierce-Point Analysis: HSGPS RMS EPE in the Garage

groups. The distributions for each group are shown in Figure 5. It can be seen that the mean fading ranges from 12 to 21 dB in different elevation groups. All elevation groups have similar distributions.

Figures 6 and 7 present the results of the satellite pierce-point analysis for the garage test. In Figure 6, the static fading data are grouped into azimuth and elevation bins of 3 deg by 3 deg to provide insight into the spatial characteristics of the test environment. The root mean square (RMS) fading value for each group is shown in the figure. The sky tracks of the satellites based on the reference station data for the same time are also shown. The receiver is clearly tracking satellites where the LOS signal is through walls and the roof. In Figure 7, the EPE values for the garage test are also binned into 3 deg by 3 deg azimuth and elevation groups, and statistics for each group are shown. The RMS EPE value is a very useful measure of the amount of error from one
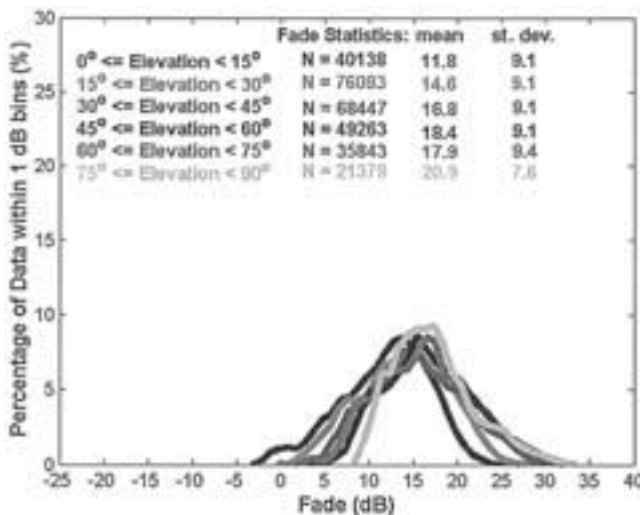
particular group. In the garage test, this value stays mainly within 30 m, and the signals presumably coming through the ceiling (if not reflected through other parts of the house) include less error than those coming through the walls.

Concrete and Steel Building

Data for the second test were collected in July 2003 for about 30 min inside the PLAN Group Navigation Laboratory, located on the top floor of the CCIT (Calgary Centre for Innovative Technology) building at the University of Calgary (see Figure 8).

Fig. 5–Fading Histogram for Each Elevation Angle Grouping in the Garage Test (N denotes the number of samples in the elevation groups.)
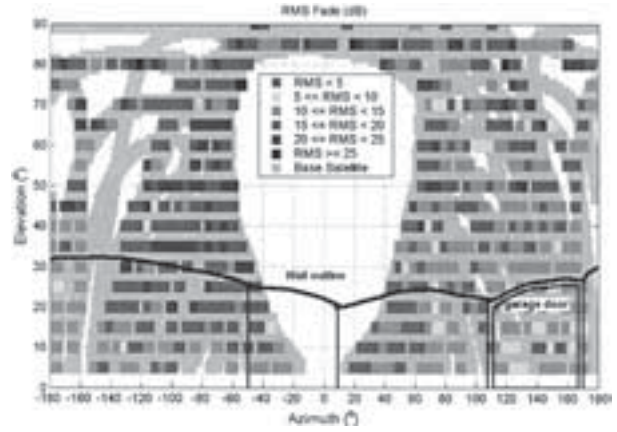

Fig. 8–CCIT Concrete and Steel Building

The test site in the Navigation Laboratory is shown in Figure 9. The HSGPS receiver was initialized using a NovAtel 600 antenna for a 20 min period on the roof, and a small patch antenna was used inside the laboratory. A NovAtel MPC system using a NovAtel 600 antenna and located on the roof of the building was used as a reference station.

To describe the characteristics of the concrete and steel building, fading conditions for one particular satellite (PRN 25) and signal fading for all satellites during the test period are presented in Figures 10 and 11, respectively. The overall fading distributions are shown in Figure 12; it can be seen that the mean fading ranges from 19 to 23 dB in different elevation groups. Figures 13 and 14 present the results of the pierce-point analysis. From Figure 13 it can be seen that the fading values vary significantly inside the concrete and steel building. Because of the design of the windows in the laboratory, GPS signals are blocked to some extent. The estimated pseudorange values in this test vary throughout the ceiling and walls between 10 and 50 m RMS, and thus it is very likely that echo-only signals are being tracked.
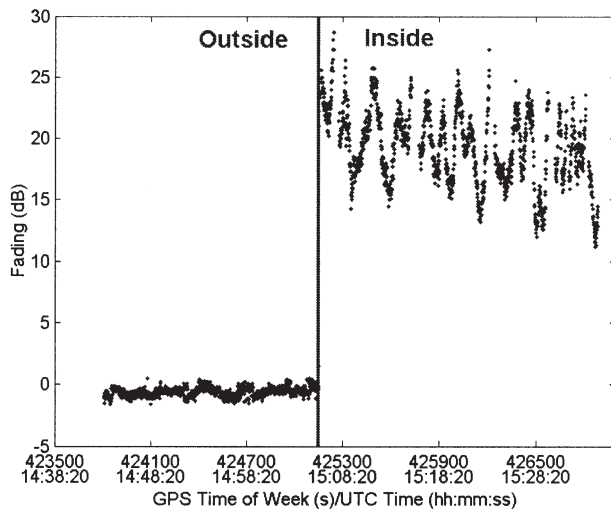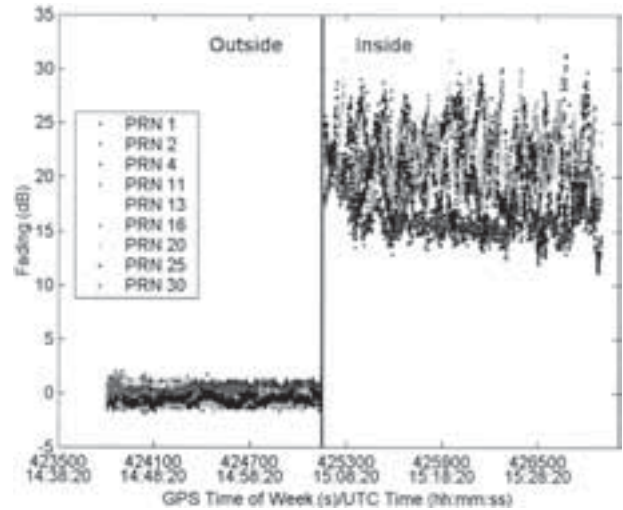

Fig. 11 – Signal Fading for All Satellites: CCIT Building

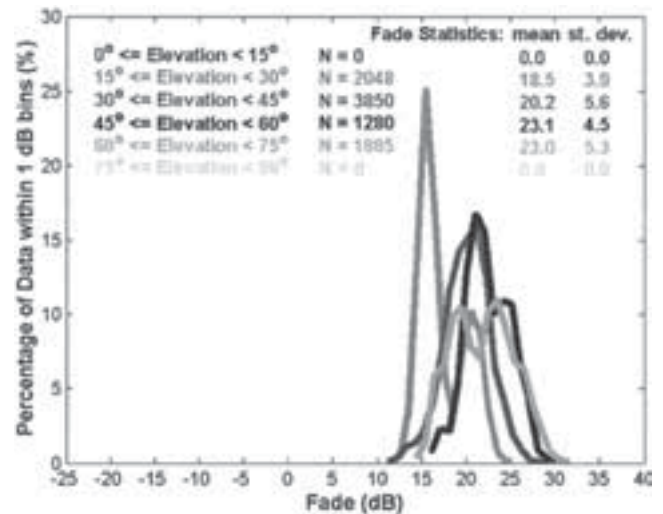*Fig. 12 – Fading Histogram for Each Elevation Angle Grouping in CCIT Building (N denotes the number of samples in the elevation groups.)*

Fig. 9 – CCIT Navigation Laboratory

Fig. 10 – Signal Fading in the CCIT Building for PRN25

EPE Frequency Analysis

In indoor tests, multipath is regarded as the dominant pseudorange error source. To assess the temporal characteristics of the multipath error of indoor environments, the power spectrums of each satellite's EPE values and the distributions of the satellite's EPE spectral power with respect to frequency can be analyzed [7]. In addition, a brief correlation analysis with plots of normalized correlation values of the pseudorange errors in time is provided.

Figure 15 presents the PRN27 EPE power spectrum for the HSGPS receiver for the indoor garage test; Figure 16 presents the PRN27 EPE power spectrum distribution with respect to frequency for the same test; and Figure 17 presents the normalized correlation values for the PRN27 EPE in time. Figures 18, 19, and 20 present the same information,
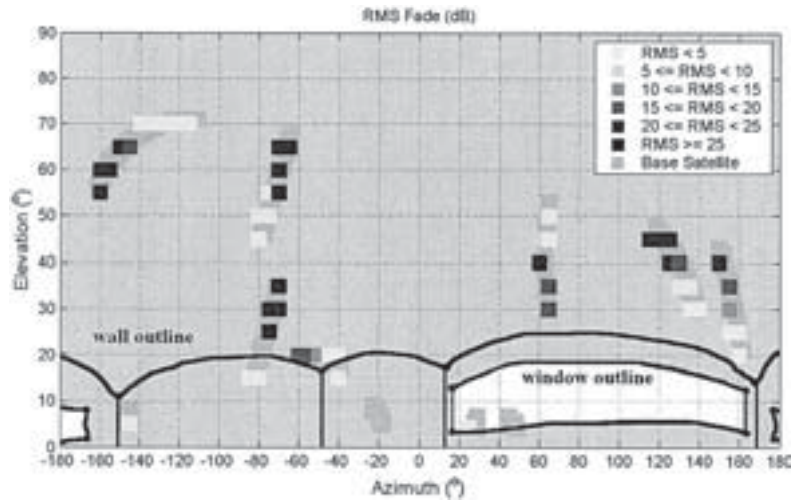
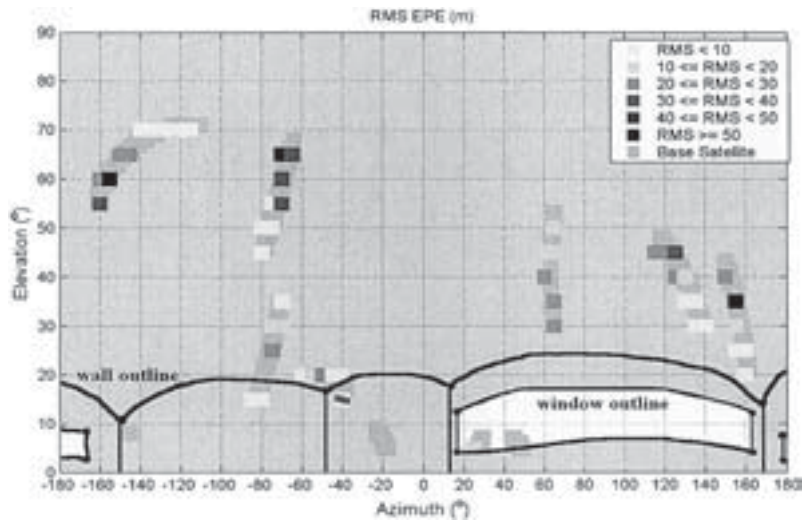*Fig. 13–Pierce-Point Analysis: HSGPS RMS Fading in CCIT Building*

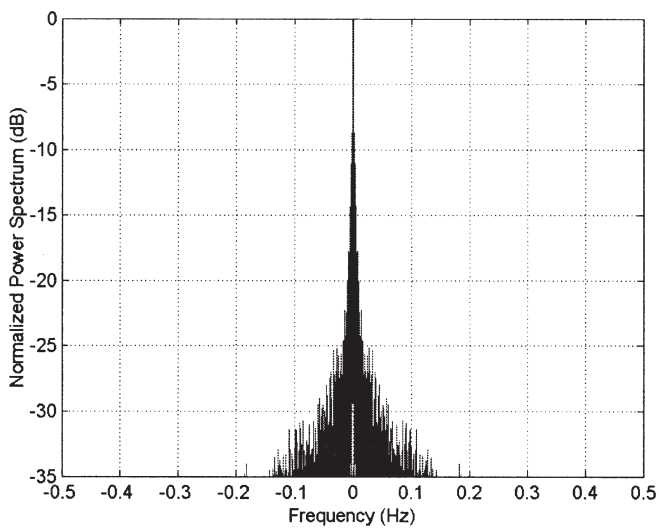*Fig. 14–Pierce-Point Analysis: HSGPS RMS EPE in CCIT Building*

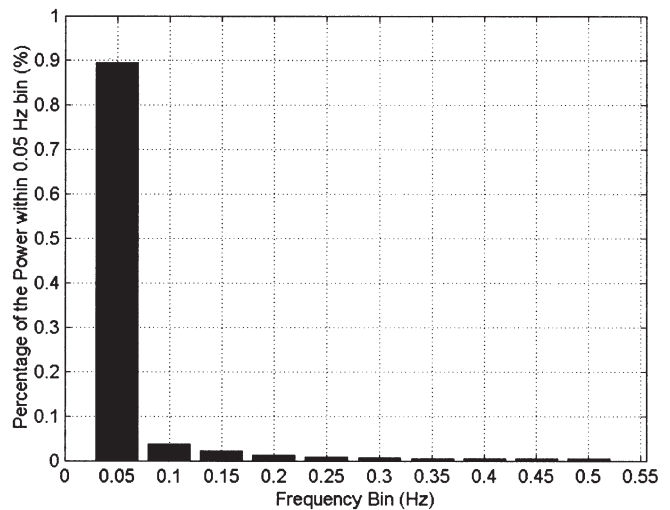*Fig. 15–PRN27 EPE Power Spectrum: Garage Test*

Fig. 16–PRN27 EPE Power Spectrum Distribution with Respect to Frequency: Garage Test
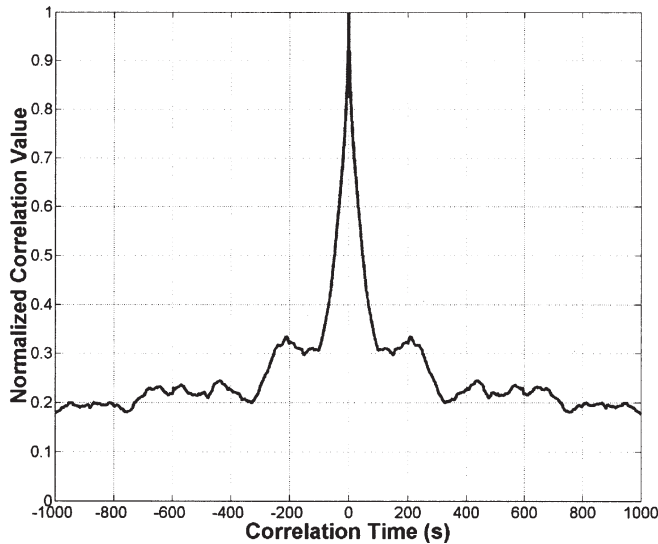
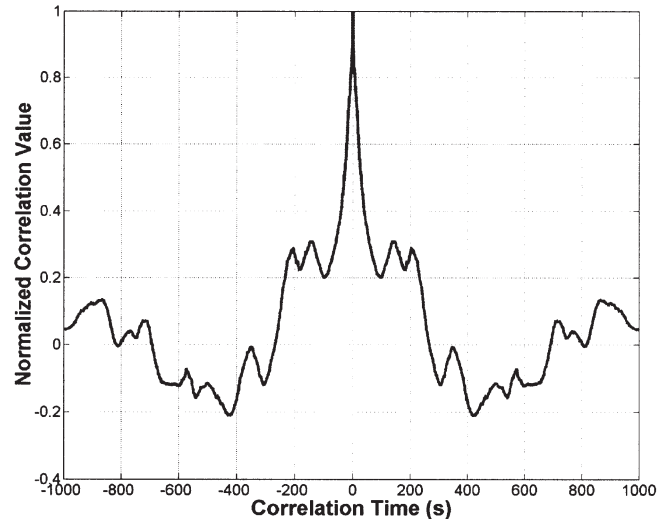Fig. 17–PRN27 EPE Normalized Correlation Values in Time: Garage Test

Fig. 20–PRN20 EPE Normalized Correlation Values in Time: Concrete and Steel Building Test
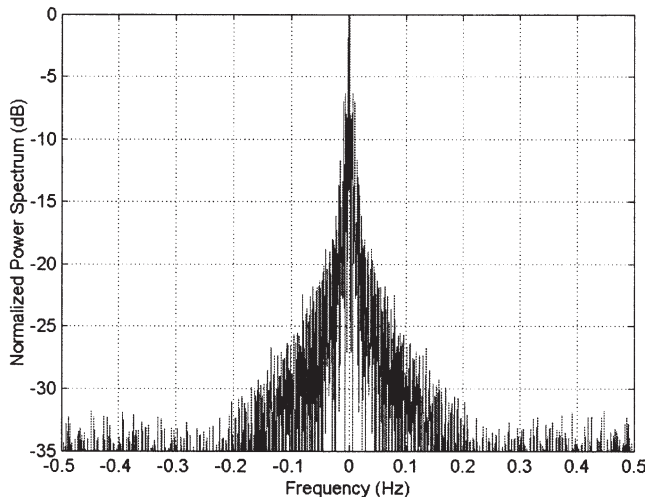
Fig. 18–PRN20 EPE Power Spectrum: Concrete and Steel Building Test
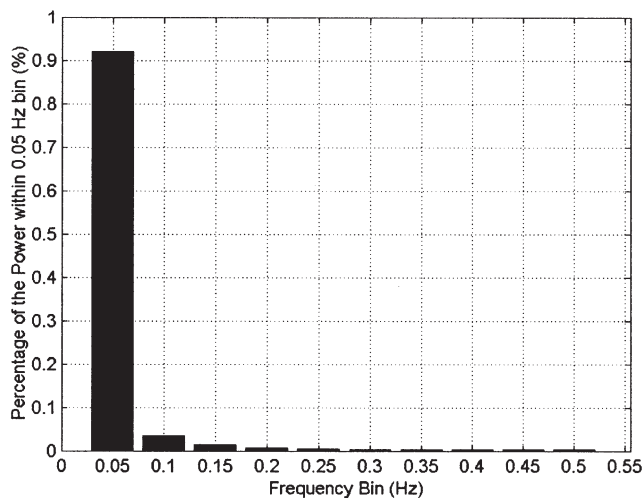
Fig. 19–PRN20 EPE Power Spectrum Distribution with Respect to Frequency: Concrete and Steel Building Test

respectively, for the CCIT building test with PRN20. For both the garage and the concrete and steel building tests, the frequencies of multipath errors were primarily (90 percent) less than or equal to 0.05 Hz, and the normalized correlation figures show a significant correlation of at least 0.6 within approximately 20 s.

MEANS TO IMPROVE HSGPS PERFORMANCE

HSGPS has many advantages compared with conventional GPS in terms of measurement and solution availability. However, degraded signals will result in low accuracy and reliability of the solution. Therefore, it is very important to improve the solution reliability when dealing with HSGPS. Assuming that the most common mode for indoor GPS positioning is static, the following methods can be applied to increase the reliability and accuracy of the solution.

Height Fixing

Height fixing is a method that results in increased measurement availability for the position computation process. Fixing is accomplished by highly constraining the variance of the height state, which results in only horizontal and time components remaining unknowns to be estimated. Height fixing is a feasible method as the height can be obtained with means other than GPS, and possibly even with better accuracy. Height can be obtained directly from a barometer [8] or from map contour details; in some map-matching schemes, GPS measurements are matched to a digital map stored as a geographic information system (GIS) database [9, 10].

Simulation-Based Noise Modeling

The relationship between the HSGPS C/N_0 and pseudorange measurement noise varies with actual signal power and thus was assessed separately using a Spirent STR6560 hardware simulator. A signal tracking threshold test was used in which the signal powers, set equally on all channels, were lowered after a 20 min warm-up period by 0.5 dB steps/min until the receiver lost track of all satellites. The EPE values and the standard deviations of the values were computed for each 1 min period with equal power. The receiver output C/N_0 with respect to the associated standard deviation is presented in Figure 21. The data exhibited a linear and an exponential trend and thus were subdivided, and appropriate functions fitted using least squares. Equations of the fitting are also shown in Figure 21 and can be used to set the variance values for the GPS measurements. The subsequent variance–covariance matrix to be used in least-squares position computation with n measurements is thus represented by the following expression:

$$\mathbf{C_1} = \begin{bmatrix} \sigma_1^2 & 0 & \cdots & 0 \\ 0 & \sigma_2^2 & 0 & \vdots \\ \vdots & 0 & \ddots & 0 \\ 0 & \cdots & 0 & \sigma_n^2 \end{bmatrix}$$

Reliability and Integrity Analysis

The increased tracking capability of HSGPS is highly beneficial in terms of solution availability and increased redundancy for reliability of navigation. At the same time, however, severe interference
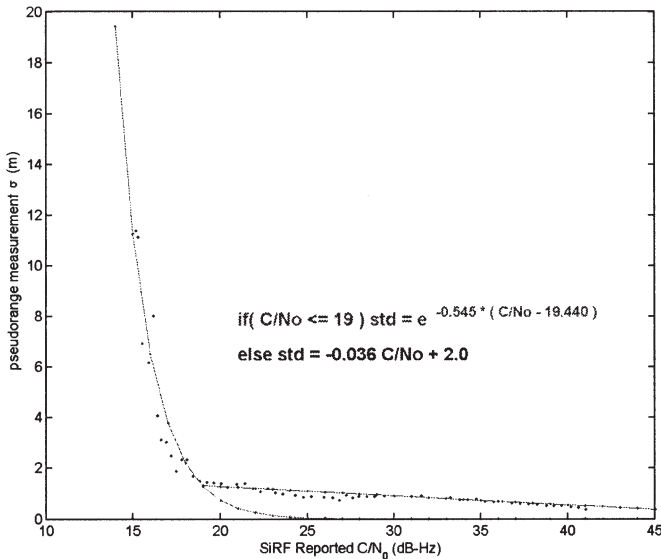

if(C/No <= 19) std = e $^{-0.545 * (C/No - 19.440)}$

else std = -0.036 C/No + 2.0

effects due to poor signal conditions of indoor environments lead to large measurement errors. Thus, reliability and integrity analysis and monitoring in terms of proper FDE becomes increasingly important in HSGPS for indoor positioning.

If redundant observations have been made, the resulting least-squares residuals can be used to test the internal consistency among measurements. The least-squares residuals are given as follows:

$$\hat{\mathbf{r}} = -\mathbf{C_{\hat{r}}}\mathbf{C_1^{-1}}\Delta\boldsymbol{\rho}$$

where the matrix $\mathbf{C_l}$ is the diagonal covariance matrix of the measurements; $\Delta\boldsymbol{\rho}$ is the misclosure vector, that is, the difference between the predicted and measured pseudorange measurements; and $\mathbf{C_{\hat{r}}}$ denotes the covariance matrix of the residuals, represented as follows:

$$\mathbf{C_{\hat{r}}} = \mathbf{C_1} - \mathbf{H}(\mathbf{H^TC_1^{-1}H})^{-1}\mathbf{H^T}$$

where $\mathbf{H}$ is the least-squares design matrix.

Reliability Testing

Global Test. A global test for detecting an erroneous and inconsistent navigation situation includes testing whether an a posteriori variance factor $\hat{\sigma}_0^2$ multiplied by the degrees of freedom $(n-p)$ is centrally chi-square distributed with a significance level of α and $n-p$ degrees of freedom [11], as represented in the following:

$$\hat{\sigma}_0^2 = \frac{\hat{\mathbf{r}}^T\mathbf{C_1^{-1}}\hat{\mathbf{r}}}{n-p}$$

$$\sigma_{0,\text{ threshold}}^2 = \frac{\chi_{\alpha,\,n-p}^2}{n-p}$$

$$H_0 : \hat{\sigma}_0^2 \leq \hat{\sigma}_{0,\text{ threshold}}^2 \text{ (No integrity failure)}$$

$$H_a : \hat{\sigma}_0^2 > \hat{\sigma}_{0,\text{ threshold}}^2 \text{ (Integrity failure)}$$

The parameter n denotes the number of satellites tracked, p denotes the number of parameters being estimated, and the significance level α denotes the probability of a good observation being rejected. If the global test fails, i.e., if a null hypothesis H_0 denoting a fault-free situation must be rejected, outliers are assumed to be included in the measurements [12], and some action should be taken. Further examination of the residuals with a local test could result in blunder localization and elimination.

Local Test. The least-squares residuals can be standardized as follows:

$$w_i = \left| \frac{\hat{r}_i}{\sqrt{(\mathbf{C_{\hat{r}}})_{ii}}} \right|, \quad i = 1 : n$$

where i denotes the i-th observation. With the assumption that only one blunder may be present in the set of observations, consecutively all residuals w_i can be statistically tested to detect that blunder [13].

The null hypothesis $H_{0,i}$, which represents the situation in which the i-th residual is unbiased, is tested against an alternative hypothesis $H_{a,i}$, which represents the case in which the i-th residual is biased, as follows:

$$H_{0,i}: w_i \leq n_{1-\frac{\alpha}{2}} \quad \text{(measurement i acceptable)}$$

$$H_{a,i}: w_i > n_{1-\frac{\alpha}{2}} \quad \text{(measurement i erroneous)}$$

The underlying assumption is that the residuals w_i are normally distributed with zero expectation in the unbiased case [14]. The measurement with the largest residual exceeding the threshold is regarded as the outlier, and that measurement is excluded from the navigation solution [15, 16]. Thus, the k-th observation is suspected to be erroneous when

$$w_k \geq w_i \, \forall i \quad \wedge \quad w_k > n_{1-\frac{\alpha}{2}}$$

The assumption of a single blunder is not always valid, particularly in indoor environments. Thus, as an approximation for a procedure to detect multiple blunders, the presented single-blunder test can be applied recursively. Whenever a blunder is detected, the test is repeated on the subsample remaining after deletion of the blunder until no more outliers are found in the navigation situation [17, 18]. This recursive residual checking procedure based on the single-blunder local test is presented in Figure 22.

However, the least-squares procedure tends to extend a blunder and particularly many blunders into all the residuals. Hence, wrong measurements could be marked as erroneous in the sequential local test. Especially in large- or multiple-blunder situations, the local test is too sensitive and may lead to many false blunder alarms [19]. Another procedure for multiple-blunder situations is thus needed apart from the sequential local test to avoid unnecessary false exclusions.

Fault Detection and Exclusion

An FDE scheme that combines the global and the sequential local tests is presented in Figure 23. However, particularly in the epoch-by-epoch position calculation, every available indoor measurement is vital to the solution geometry. Thus in some cases, incorporating an erroneous measurement into the position solution may be a better alternative than excluding that measurement in terms of ensuring an acceptable observation geometry. Thus if excluding a measurement with a supposed blunder would lead to a poor horizontal dilution of precision (HDOP) value, that measurement should not be excluded, and the position solution obtained with the measurements at hand should be provided to the user, albeit with a warning.

An FDE scheme that combines the global test, the local test, and the geometry check described above based on the HDOP value is presented in Figure 24. In the decision on whether to exclude a measurement k, the HDOP for the remaining observations is chosen to be acceptable if it is smaller than 5 in the epoch-by-epoch case and smaller than 1 in the batch-processing case, where more measurements are used, as described later. The HDOP threshold values to ensure acceptable horizontal geometry were chosen on an experimental basis, but they can be changed. Both the sequential FDE scheme in Figure 23 and the FDE scheme including a geometry check in Figure 24 can

Fig. 23 – FDE Scheme with Global and Sequential Local Tests

Fig. 22 – The Sequential Local Test

Fig. 24 – FDE Scheme with Global Test, Local Test, and a Geometry Check before Exclusion

provide the user with a warning of an unreliable position solution in case the final global test fails.

Least-Squares Batch Processing for Static Mode

The problem with epoch-by-epoch HSGPS positioning is the lack of available observations in each epoch, which results in limitations for reliability testing. Assuming that a common user mode is static in indoor GPS positioning, batch processing can be applied. Batch processing in this context refers to the use of measurements from multiple epochs for the least-squares position calculation process. Compared with the single-epoch case, batch processing gathers more 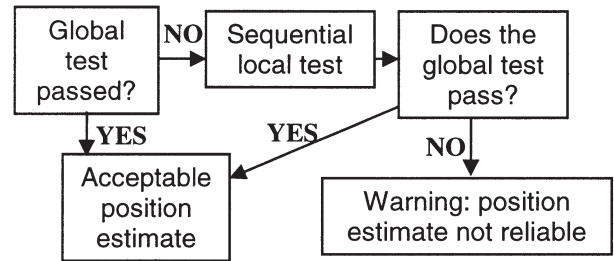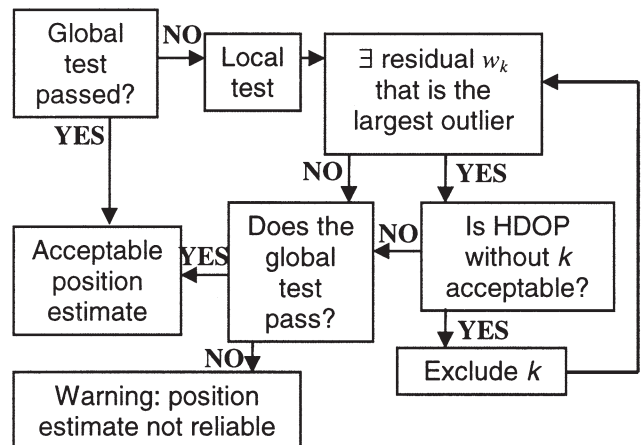measurements to estimate the unknown parameters. Therefore, the number of redundant measurements is higher, and the result is a more reliable and more accurate solution, though averaged over many epochs. Obtaining measurements from many epochs also helps improve the solution geometry and leads to better DOP values. Thus, batch processing is a highly effective method, although it can be employed only when the user is in a static mode. If the motion state of the user is not already known, some additional sensor system, such as a microelectromechanical systems (MEMS), can be applied to detect the motion state and identify the user mode [20].

In a batch implementation with N epochs, the design matrix, i.e., the geometry matrix, for the least-squares calculation is constructed as follows:

$$\mathbf{H}_b = \begin{bmatrix} \frac{\partial f^{1_1}}{\partial \phi} & \frac{\partial f^{1_1}}{\partial \lambda} & \frac{\partial f^{1_1}}{\partial h} & 1 & 0 & \cdots & 0 \\ \vdots & & \vdots & \vdots & & & \vdots \\ \frac{\partial f^{1_j}}{\partial \phi} & \frac{\partial f^{1_j}}{\partial \lambda} & \frac{\partial f^{1_j}}{\partial h} & 1 & 0 & \cdots & 0 \\ \cdots \cdots & & & & & & \\ \frac{\partial f^{N_1}}{\partial \phi} & \frac{\partial f^{N_1}}{\partial \lambda} & \frac{\partial f^{N_1}}{\partial h} & 0 & 0 & \cdots & 1 \\ \vdots & & \vdots & \vdots & & & \vdots \\ \frac{\partial f^{N_m}}{\partial \phi} & \frac{\partial f^{N_m}}{\partial \lambda} & \frac{\partial f^{N_m}}{\partial h} & 0 & 0 & \cdots & 1 \end{bmatrix}_{(j+\ldots+m)\times(N+3)}$$

where ϕ denotes the latitude, λ the longitude, h the height, N the number of epochs used in the batch calculation, j the number of measurements in the first epoch, and m the number of measurement in the last epoch.

The variance-covariance matrix $\mathbf{C}_{1_b}$ in the implemented batch approach is formed by assuming measurements from a single epoch to be independent and obtaining the standard deviations of pseudorange measurement errors from the simulation-based noise-modeling equation depicted earlier in Figure 21. If it is assumed that multipath is one of the dominant error sources and that this degradation is always present in indoor applications, certain temporal multipath error correlation may be included in the batch approach.

Given the frequency domain and correlation analyses performed on the environments tested, a dominant error period of about 20 s was found. It is expected that there is strong error correlation between epochs for 1/4 of this period. In the batch variance-covariance matrix, the parameter k represents the approximate correlation coefficient that is assumed to exist between the same-satellite measurements at hand. The correlation coefficient k was chosen to decrease from 0.8 to 0.0 within the 1/4-period (5 s) of the multipath error period, and thus measurements from the same satellite in the batch processing with a one-epoch difference have a k value of 0.8, those with a two-epoch difference have a k value of 0.6, and so on. Measurements with a difference of five or more epochs are considered not to be correlated in terms of multipath error (see Figure 25). The length of the batch period, i.e., the value N, is desired to be at least the period of the approximate dominant multipath error frequency, 20 s, so that multipath errors can also decorrelate temporally to some extent, and some of the measurements may thus not be flagged as blunders. This means the solution geometry will not be adversely affected by the loss of a satellite.

The batch variance-covariance matrix is as follows:

$$\mathbf{C}_{1_b} = \begin{bmatrix} \sigma_{1_1}^2 & & \mathbf{0} & & k\sqrt{\sigma_{1_1}^2\sigma_{2_1}^2} & & \ddots \\ & \ddots & & & & & \\ \mathbf{0} & & \sigma_{1_j}^2 & & & & \\ k\sqrt{\sigma_{1_1}^2\sigma_{2_1}^2} & & & \sigma_{2_1}^2 & & \mathbf{0} & \\ \ddots & & & & \ddots & & \\ & & & \mathbf{0} & & \sigma_{2_s}^2 & \\ & & & & & \cdots & \\ & & & & & & \sigma_{N_1}^2 & \mathbf{0} \\ & & & & & & \mathbf{0} \ddots \\ & & & & & & & \sigma_{N_m}^2 \end{bmatrix}$$

Fig. 25 – Temporal Correlation Coefficient for Multipath Errors

After obtaining the batch design matrix $\mathbf{H_b}$ and the batch measurement variance-covariance matrix $\mathbf{C_{1_b}}$, a standard least-squares estimation procedure can be applied.

TEST RESULTS

Data processing in the following analyses is based on the use of a modified version of a C³NAVG²™ software package developed by the PLAN group at the University of Calgary. In the following, the results for the garage test and the concrete and steel building test are presented using the different improvement approaches described in the previous section. The analysis is focused on the effects of the reliability testing schemes and the batch processing on position accuracy and reliability. In the least-squares data processing, differential corrections, height fixing, and simulation-based noise modeling are always used. The significance level α used in obtaining the thresholds for reliability testing was chosen as 0.1 percent. Figures 26, 27, and 28 present the effects of the FDE reliability schemes on the position solution in the garage test, and Figures 29, 30, and 31 present the same information for the CCIT building test.

Sequential reliability testing increases the horizontal position error because of the exclusion of measurements that are essential to the solution geometry, and is thus not an applicable FDE scheme for indoor positioning. The reliability testing scheme including the geometry check overcomes to some extent the problem of excluding measurements vital to an acceptable solution, and is recommended for weak-environment positioning because of its contribution in providing reliability information. The capability to warn the user in case of final global test failure or lack of redundancy to
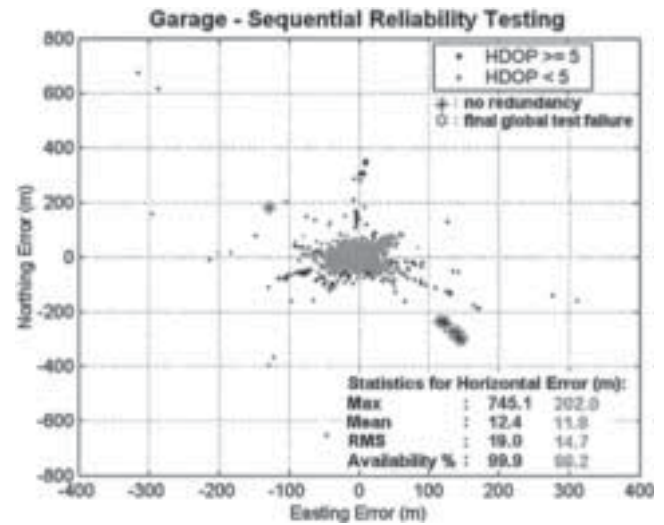
Fig. 27–*Epoch-by-Epoch Result with FDE Scheme Presented in Figure 23: Garage Test*
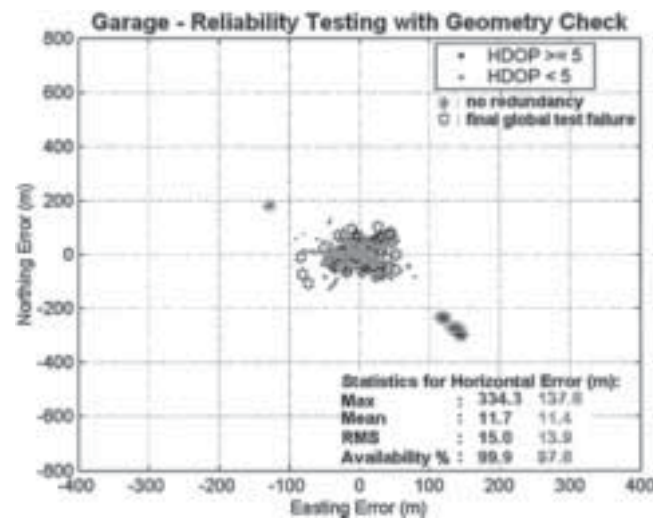
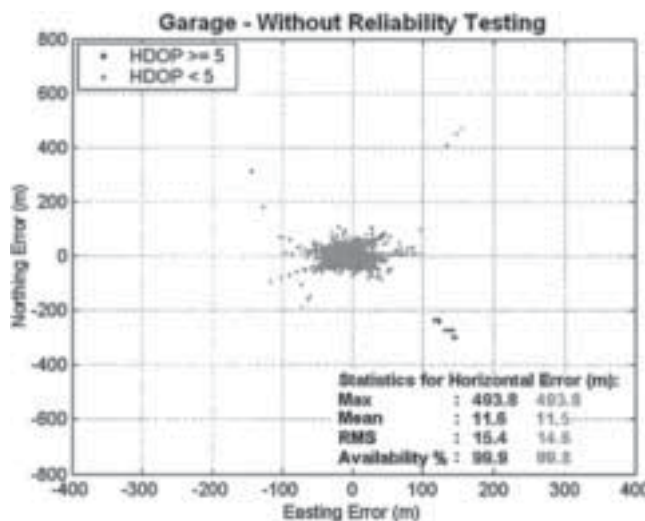Fig. 28–*Epoch-by-Epoch Result with FDE Scheme Presented in Figure 24: Garage Test*

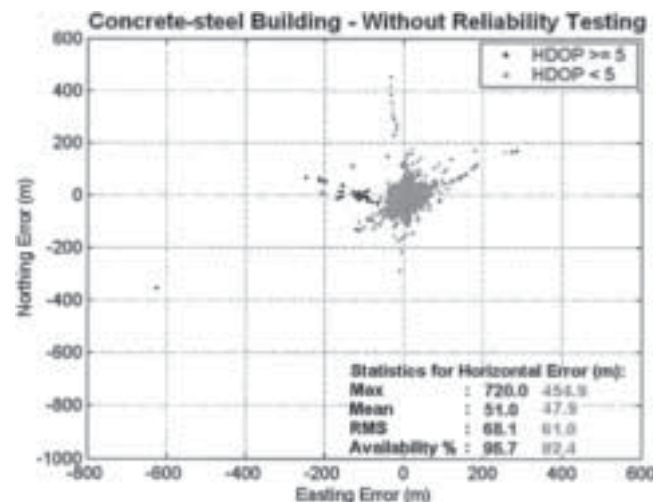Fig. 26–*Epoch-by-Epoch Result without Reliability Testing: Garage Test*

Fig. 29–*Epoch-by-Epoch Result without Reliability Testing: CCIT Building Test*
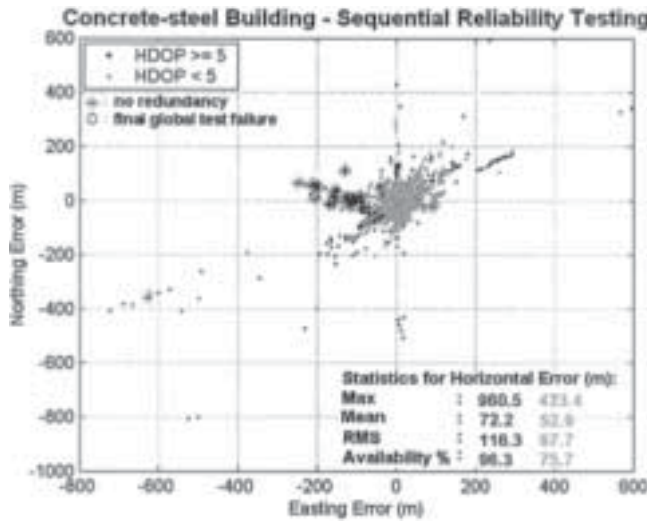
Fig. 30–*Epoch-by-Epoch Result with FDE Scheme Presented in Figure 23: CCIT Building Test*
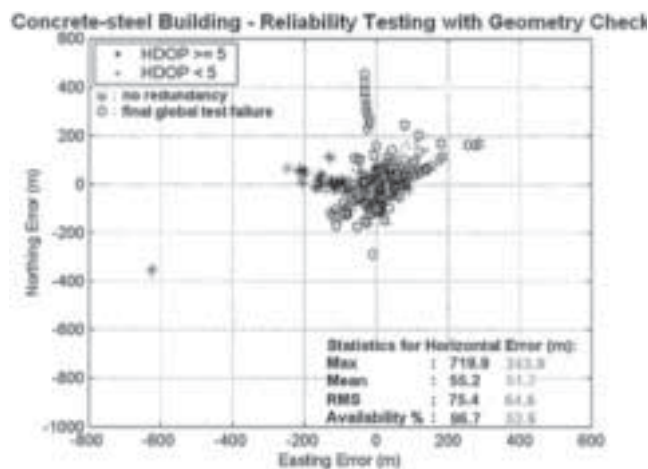

Fig. 31–*Epoch-by-Epoch Result with FDE Scheme Presented in Figure 24: CCIT Building Test*

provide reliability testing is implemented in both schemes, and offers additional important information on overall performance.

In Figure 28, for example, the poor solutions are accompanied by a warning of the lack of reliability and availability, with a asterisk, a star, and a darker dot representing the lack of redundancy, a final global test failure, and an HDOP value larger than 5, respectively. In the statistics, the darker values represent the horizontal error information for all available solutions, while the lighter values denote the information for solutions considered reliable. The reliable solutions are defined as those with no warnings and HDOP values smaller than 5, and result in lower availability but better accuracy.

Consequently, in the 12 h garage test, the mean of the horizontal error is approximately 10 m; when reliability testing with a geometry check is used, the accuracy improves slightly, and reliability warnings

are provided. In the 30 min CCIT building test, the mean of the horizontal error is approximately 50 m; when reliability testing is used, the statistics show no improvement in accuracy, but reliability warnings provide valuable additional information.

The contribution of a 20 s batch approach to further improving performance is now assessed. In Figures 32 and 33, the performance of batch processing is compared with the epoch-by-epoch solutions of the garage test and the concrete and steel building test, respectively. In the statistics, the darkest values present the horizontal error information for all available epoch-by-epoch solutions, while the light grey values denote the information for all available batch solutions. In both tests, the statistics for the batch approach show a significant improvement in solution accuracy. This improvement can be concluded from the decrease in the mean and the RMS of the horizontal errors. However, reliability testing failed to improve the solution accuracy in some batch cases because of
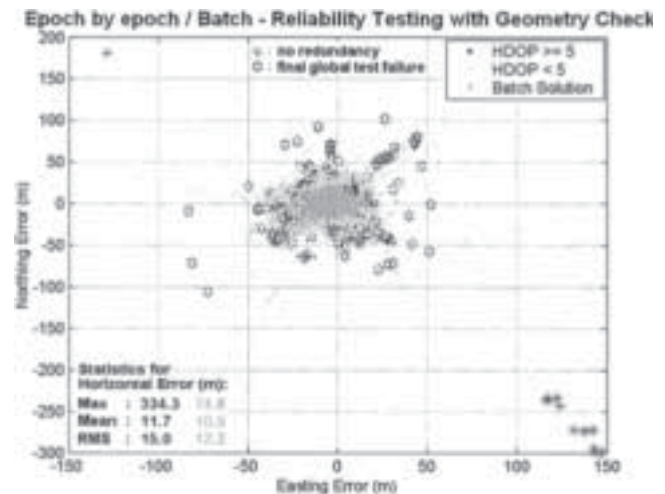

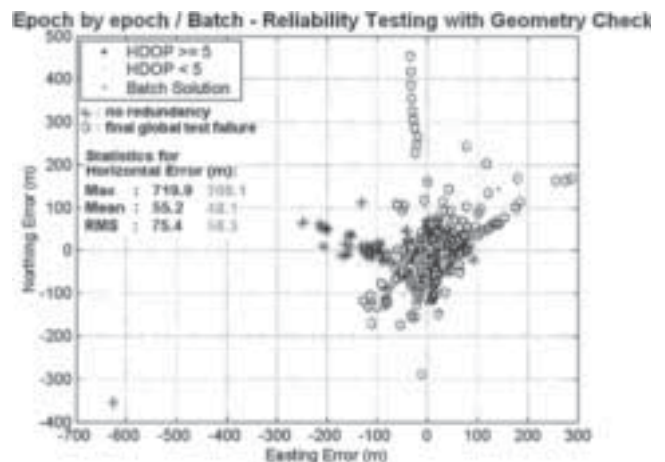Fig. 32–*Batch Result with FDE Scheme Presented in Figure 24: Garage Test*

Fig. 33–*Batch Result with FDE Scheme Presented in Figure 24: CCIT Building Test*

poor geometry and multiple errors, making correct exclusion difficult and still resulting in significant maximum error values.

In Figures 34 and 35, batch processing solutions with and without reliability testing, respectively, are compared for the garage and CCIT building tests to analyze the effect of FDE in the batch approach. When one applies reliability testing including the geometry check, which is concluded to be the more applicable of the FDE schemes for indoor conditions where redundancy is limited, the horizontal error is decreased, and some outliers are excluded or flagged. Thus the accuracy and reliability are improved.

The effect of applying temporal multipath error correlation to the batch processing approach is presented in Figures 36 and 37.

Fig. 36 – Effect of Including the Temporal Multipath Error Correlation: Garage Test

Fig. 34 – Comparing Batch Results with and without Reliability Testing: Garage Test

Fig. 37 – Effect of Including the Temporal Multipath Error Correlation: CCIT Building Test

Fig. 35 – Comparing Batch Results with and without Reliability Testing: CCIT Building

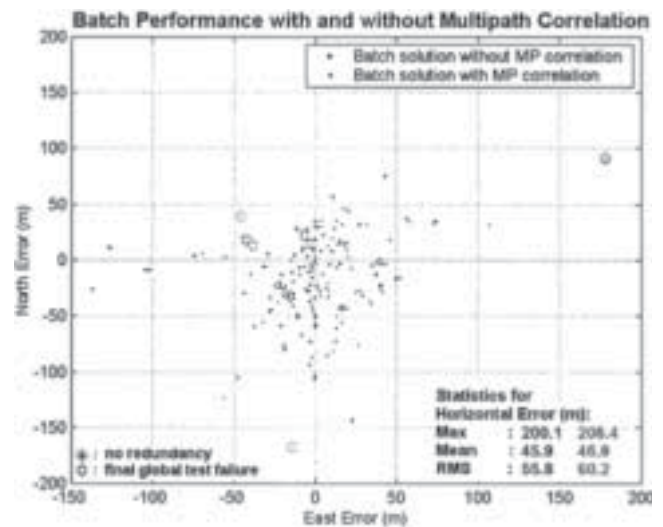When the temporal multipath correlation is included, the statistics show slightly worse performance. However, only two datasets were tested, and therefore this result is not conclusive. Including the temporal multipath correlation, moreover, is a matter of taking into account the multipath effect itself and constraining the least-squares batch adjustment accordingly. A major limitation, of course, is that multipath is not normally distributed.

CONCLUSIONS

HSGPS increases solution availability in indoor conditions. However, severe interference effects due to poor signal conditions lead to large measurement errors. Therefore, reliability and accuracy improvement methods including statistical FDE are required.

The methods presented in this paper offer some possibilities for enhancing the reliability of indoor HSGPS. The environments examined show significant signal fading—typically 15 dB in RMS and up to 30 dB as a maximum value. The pseudorange errors in the test environments are often greater than 30 m. Therefore, multipath effects and echo-only signal tracking clearly induce significant measurement errors.

In conclusion, sequential reliability testing (Figure 23) is not suitable for indoor environments because it excludes measurements too vital to the solution geometry. The FDE reliability testing scheme including the geometry check (Figure 24) overcomes this limitation to some extent, improves accuracy, and provides reliability warnings. However, both FDE schemes suffer from false exclusions due to the low measurement redundancy level and the existence of multiple blunders that obviate the underlying assumptions. Still, the traditional aviation-related statistical consistency tests aimed at FDE are essential in indoor environments to improve overall reliability. The batch processing approach is highly beneficial for static indoor HSGPS positioning in providing overall significant improvements in accuracy, reliability, and solution geometry.

For future work, certain measurement subset tests with the a posteriori variance factor as the test statistic could be conducted as a more robust FDE scheme for dealing with multiple-blunder situations. In addition, the potential adaptive use of DOP values in the sequential reliability testing scheme will be studied. The temporal multipath error correlation effect in the batch computation should be further studied as well. Moreover, extending the batch approach, along with the other improvement methods, to kinematic user mode and using external aiding (self-contained sensors) should be examined. The use of a Kalman filter with constraints would also provide reliability improvements, but at the cost of smoothing and overshooting effects (in the case of a pedestrian, effective trajectory constraints are very limited).

REFERENCES

1. Brown, R. G., *A Baseline GPS RAIM Scheme and a Note on the Equivalence of the Three RAIM Methods*, Proceedings of The Institute of Navigation's National Technical Meeting, San Diego, CA, January 27–29, 1992, pp. 127–38.

2. Van Graas, F. and J. L. Farrell, *Baseline Fault Detection and Exclusion Algorithm*, Proceedings of The Institute of Navigation's Annual Meeting, Cambridge, MA, June 21–23, 1993, pp. 413–20.

3. MacGougan, G., *High-Sensitivity GPS Performance Analysis in Degraded Signal Environments*, M.Sc. Thesis, The University of Calgary, UCGE Report 20176, 2003, p. 243.

4. Van Diggelen, F. and C. Abraham, *Indoor GPS, The No-Chip Challenge*, GPS World, Vol. 12, No. 9, September 2001, pp. 50–58.

5. SiRF Technology, Inc., *SiRFXTrac Product Information*, available February 2004, http://www.sirf.com/products-sirfxtrac.html.

6. ICD200C, *GPS Interface Control Document*, ARINC Research Corporation, NAVSTAR GPS Space Segment/Navigation User Interfaces, 2000, IRN-200C-004.

7. Lachapelle, G., O. Julien, G. MacGougan, M. E. Cannon, and S. Ryan, *Ship GPS Multipath Detection Experiments*, Proceedings of The Institute of Navigation's Annual Meeting, Albuquerque, NM, June 23–25, 2003, pp. 217–29.

8. Parkinson, B. W. and J. J. Spilker, editors, *Global Positioning System: Theory and Applications*, Vols. 1 and 2, AIAA Inc., 1996, p. 643 and 793.

9. Basnayake, C. and G. Lachapelle, *Accuracy and Reliability Improvement of Standalone High Sensitivity GPS Using Map Matching Techniques*, Proceedings of The Institute of Navigation's Annual Meeting, Albuquerque, NM, June 23–25, 2003, pp. 209–16.

10. Mezentsev, O., J. Collin, and G. Lachapelle, *Vehicular Navigation in Urban Canyons Using a High Sensitivity GPS Receiver Augmented with a Medium-Grade IMU*, Proceedings of 10th Saint Petersburg International Conference on Integrated Navigation Systems, St. Petersburg, Russia, May 26–28, 2003, pp. 64–70.

11. Caspary, W. F., *Concepts of Network and Deformation Analysis*, UNSW, Australia, School of Surveying, Monograph, 11, 1988, p. 183.

12. Kuang, S., *Geodetic Network Analysis and Optimal Design*, Ann Arbor Press, Chelsea, MI, 1996, p. 368.

13. Leick, A., *GPS Satellite Surveying*, John Wiley & Sons Inc., 2nd Edition, 1995, p. 560.

14. Ryan, S., *Augmentation of DGPS for Marine Navigation*, Ph.D. Thesis, The University of Calgary, UCGE Report 20164, 2002, p. 248.

15. Kelly, R. J., *The Linear Model, RNP, and the Near-Optimum Fault Detection and Exclusion Algorithm*, NAVIGATION, Journal of The Institute of Navigation, Vol. 5, 1998, pp. 227–59.

16. Teunissen, P. J. G., *Quality Control and GPS*, Chapter 7 in GPS for Geodesy, 2nd Edition, P. J. G. Teunissen and A. Kleusberg, editors, Springer, New York, NY, 1998, p. 650.

17. Hawkins, D. M., *Identification of Outliers*, Chapman & Hall, London/New York, NY, 1980, p. 188.

18. Petovello, M. G., *Real-Time Integration of a Tactical-Grade IMU and GPS for High-Accuracy Positioning and Navigation*, Ph.D. Thesis, The University of Calgary, UCGE Report 20173, 2003, p. 242.

19. Lu, G., *Quality Control for Differential Kinematic GPS Positioning*, M.Sc. Thesis, The University of Calgary, UCGE Report 20042, 1991, p. 103.

20. Collin, J. and J. Käppi, *Navigating the City*, Galileo's World Magazine, Advanstar Communications, Vol. 4, No. 1, 2002, pp. 21–29.